



Solid Particle Erosion Behaviour of Plasma-Sprayed (WC–Co)/ (Cr₃C₂–NiCr) Coatings

G. Madhu Sudana Reddy¹ · S. Ramesh² · Gajanan Anne³ · M. R. Ramesh⁴ · T. Nageswara Rao⁵ · Pradeep Patil⁵

Received: 11 October 2021 / Revised: 24 November 2021 / Accepted: 4 January 2022 / Published online: 11 February 2022
© The Author(s), under exclusive licence to Springer Nature Switzerland AG 2022

Abstract

This study reports the high-temperature erosion behaviour of plasma-sprayed 35% (WC–Co)/65% (Cr₃C₂–NiCr) coating on MDN-420 alloy. Plasma spray coatings have always played a pivotal role in enabling industries to combat problems of premature degradation of components that operate in harsh environments. (WC–Co) + (Cr₃C₂–NiCr) coating is investigated for erosion under various laboratory-simulated conditions. Coating surface is characterized by using an optical microscope, scanning electron microscope (SEM), and X-ray diffraction (XRD). Porosity, microhardness, surface roughness, and adhesion strength of the coating are measured. The solid particle erosion test is conducted at the temperatures of 300 °C, 500 °C and 700 °C with the impact angles of 30° and 90° by using Al₂O₃ as an erodent in the hot air jet erosion testing machine. The optical profilometer is used to evaluate the erosion volume loss of the coated and uncoated samples. It is observed that erosion resistance of the substrate is found to be higher than the coating at the different test temperatures. As the temperature increases, the erosion resistance of the coating is also increased at all the temperatures for both impact angles of 30° and 90°. The eroded coating surface morphology reveals that the generalized behaviour of the coating is ductile in nature.

Keywords MDN-420 alloy · Plasma spray · (WC–Co)/Cr₃C₂–NiCr · Metal matrix composite · Erosion

1 Introduction

Erosion is recognized as one of the serious problems in the coal-based thermal power plants in our country. The coal which is used in these power plants has the large amount of ash which consisting of hard quartz [1], which is main variable for the erosion to occur. The solid particle erosion is one of the important material degradation mechanisms which also occurs in high-temperature environments like

jet engine parts, steam, gas turbines coal pipe lines and offshore oil. Thermal power plants are one of the most highly corroded and eroded component sectors, resulting in large losses [2–4]. To prevent material deterioration, a number of strategies or techniques have been widely used. Thermal spraying technique is one of the most challenging approach that has attracted a lot of attention due its adaptability in spraying any form of powder to any type of substrate, preventing material degradation [5]. The different types of coating techniques are available such as flame spray, high velocity oxy fuel, cold spraying, detonation gun, plasma spray etc. [6]. Due to its ease of use, high deposition speeds, low substrate temperature and economic viability, plasma spraying is regarded as the most efficient and cost-effective technique for preparing coatings for high-temperature applications. The coating material is inserted as powder into a high-temperature plasma jet in the plasma-spraying process. The particle will melt and speed up as it reaches the substrate [7]. When the molten particle is pressed or flattened and quenched on the substrate during impact, Splatt borders, layered microstructure, pores and micro-cracks are created [8]. The plasma-spraying method provides the coating with thickness of few to hundreds of micrometres

✉ S. Ramesh
ramehs.rvitm@rvei.edu.in

¹ Department of Mechanical Engineering, Oxford College of Engineering, Bangalore 560068, India

² Department of Mechanical Engineering, RV Institute of Technology and Management, Bangalore 560076, India

³ Department of Mechanical Engineering, Shri Madhwa Vadiraja Institute of Technology and Management, Udupi 574115, India

⁴ Department of Mechanical Engineering, National Institute of Technology Karnataka, Surathkal 575025, India

⁵ Department of Mechanical Engineering, Gitam University, Bangalore 560065, India

with good-quality adherent coating [9]. The (WC–Co)/Cr₃C₂–NiCr coatings are mainly designed for erosion and corrosion resistance at elevated temperatures or at a room temperature in aggressive wear and corrosive environments [10]. The reinforced hard phases like Cr₃C₂, Cr₂O₃, WC, TiC, TiO, TiN, and CeO₂ [10] will greatly boost the erosion resistance of these coatings. (WC–Co) + (Cr₃C₂–NiCr) coating is an excellent replacement to the hard oxide Cr₂O₃. This cermet coating consists of WC or Cr C particles embedded in a metal binder, which can be a pure metal or a mixture consisting of Ni, Cr and Co. WC–Co and CrC–NiCr systems constitute two main carbide materials used in the plasma spray processes in order to improve the wear or erosion resistance and decrease the friction coefficient between various sliding components. Hence, (WC–Co) + (Cr₃C₂–NiCr) coatings are widely used in high-temperature wear resistance applications in aggressive environments such as oil and gas, aerospace and power generating industries [11–13]. Furthermore, the understanding of the mechanism of (WC–Co)/Cr₃C₂–NiCr coating in the erosion behaviour is one of the most challenging and interesting tasks.

In the present investigation, the atmospheric spray process is used to deposit the 35% (WC–Co) + 65% (Cr₃C₂–NiCr) coating on special steel alloy MDN-420 alloy. Erosive behaviour of the coated and uncoated samples is investigated at the temperatures of 300 °C, 500 °C and 700 °C with impact angles of 30° and 90° in the hot air jet erosion testing machine. The alumina (Al₂O₃) is used as an erodent. To evaluate the erosion loss of the coating and substrate, weight and volume loss approaches are used. The advanced characterization techniques like SEM and XRD are carried out to investigate the erosion mechanism and behaviour of the coating. In this study, the special steel alloy (MDN-420) is used as the substrate due its excellent oxidation, corrosion and erosion resistance. (WC–Co)/Cr₃C₂–NiCr coating was developed specifically for the purpose of its excellent corrosion, erosion resistance and also having the high hardness, high melting point and strength unto a maximum operating temperature of 900 °C.

2 Experimental Procedure

2.1 Substrate Materials and Development of Coating

MDN-420 alloy is procured from the MDNL, Hyderabad. The specimens were cut with the dimensions of

25 × 25 × 5 mm from the alloy sheet by using laser technology. The commercially available (WC–Co)/Cr₃C₂–NiCr powder is used to coat on special steel alloy MDN-420 alloy and chemical composition of the coated surface is analysed using Optical Emission Spectroscopy and is tabulated in Table 1. (WC–Co) + (Cr₃C₂–NiCr) coating provides possible protective scale, with erosion resistance for long-term stability and also resistance of cracking, mechanical or thermal stresses induced during the operation of the component. This (WC–Co) + (Cr₃C₂–NiCr) coating is an appropriate, which is suitably designed for erosion resistance, which would be an optimum solution (WC–Co) + (Cr₃C₂–NiCr) coating is an excellent replacement to the hard oxide Cr₂O₃. A feedstock powder particle exhibits the spherical shape morphology, which provides excellent stability and fluidity during spraying. The standard particle size distribution is found to be -45 + 15 μm with the mass fraction of 35% (WC–Co) + 65% (Cr₃C₂–NiCr).

2.2 Coating Formulation and Characterization

Plasma spray process (M/s SSTPL, Bangalore, India) of METCO USA 3 MB machine system is used to deposit the 35% (WC–Co) + 65% (Cr₃C₂–NiCr) powder on the MDN-420 alloy. Before coating, the substrate is finely grit blasted by using the Al₂O₃ powder of 125–150 μm size to promote the better quality and adhesion between the coating and substrate. The powder is supplied by a feeder during the plasma-spraying process, which is mixed with the argon gas flowing through the compressor at the selected pressure. The mixture is attracted to the plasma stream, where it melts and is deposited on the substrate. The coating is deposited at a rate of 10–15 m per pass, with the 40–50% efficiency. The produced coating's thickness is measured by scanning electron microscopy analysis. The micrograph of the coating thickness and EDS is shown in Fig. 1. The coating porosity is measured by using the optical microscope supported with the (ARTRAY, AT 130, and JAPAN). The coating phases are examined and investigated using the (DX, GE-2P, JEOL, JAPAN) XRD (X-ray diffractometer). The details of the plasma spray parameters are summarized in Table 2.

Maximum coating porosity value is calculated by using image analysis software (Biovis image analyser, ARTRAY, AT, 130 Japan). As per the ASTM C-633-13 standards, the bond strength of the coating is measured by carrying out the pull-off test. The coated sample is glued with the counter block by using the EC-1386 Epoxy Adhesive (3M-Scotch weld). The alignment is cured in the silicon carbide furnace

Table 1 Chemical compositions of MDN-420 alloy

Element	C	Mn	Si	S	P	Cr	Ni	Mo	Fe
Weight percentage (%)	0.19	0.71	0.47	0.003	0.017	13.79	0.50	0.03	Bal

Fig. 1 SEM images of **a** morphology of (WC–Co) + (Cr₃C₂–NiCr) powder, **b** magnified image

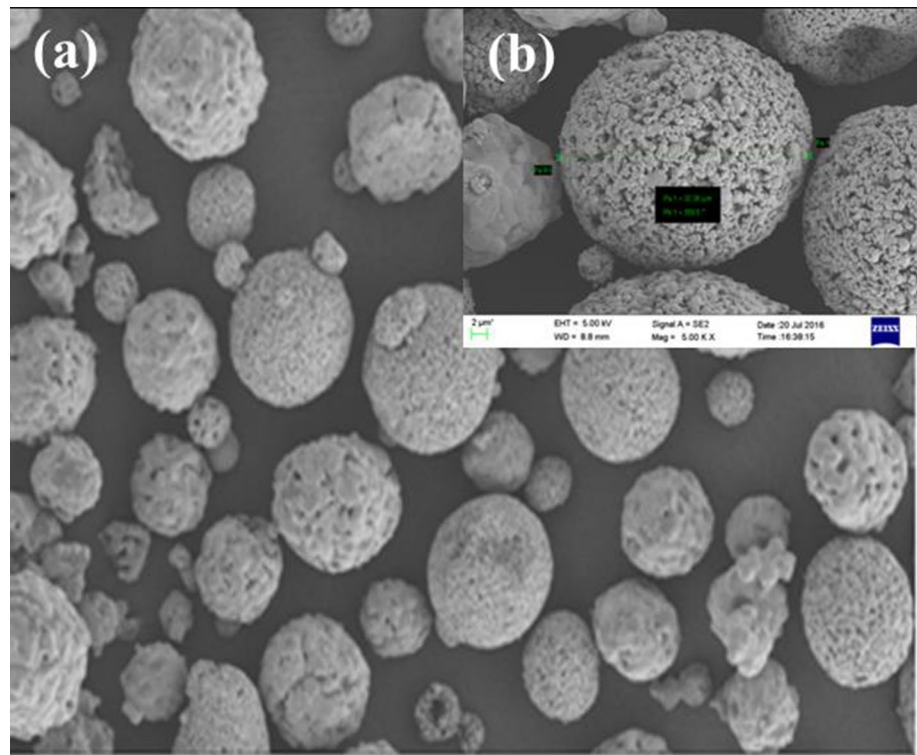


Table 2 Plasma spray-coating process parameters

Pressure of H ₂ gas	0.35 Mpa
Pressure of Ar gas	0.6–0.7 Mpa
Flow rate of H ₂ gas	5–7 l/min
Flow rate of Ar gas	40 l/min
Electricity	1350 A
Potential difference	60–70 V
feed rate (power)	50–60 g/min
SOD	100–125 mm

at the temperature of 150–175 °C for about 2 to 3 h. After curing, the UTM system (M/s SHTM, AG–X Plus, Japan) is used to perform a pull-off test at a strain rate of 0.5 mm/min.

2.3 Erosion Studies

Schematic representation of the air jet erosion tester is shown in Fig. 2. The erosion studies on solid particles were investigated as per the ASTM G76-13 standard by using air jet erosion tester (DIPVL, TR-471-800, and Bangalore, India). The alumina powder is used to conduct the erosion test on uncoated and coated samples. The mixed chamber unit is fed with the Al₂O₃ erodent with a feed rate of 2 g/min, get mix up with the hot air impinges on to the substrate with a velocity of 30 m/s. By modifying the sample holder's direction, the impact angle for the specimen can be changed.

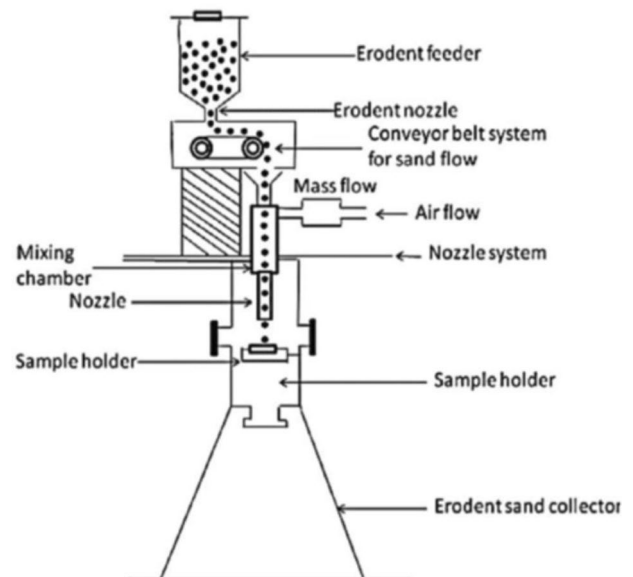


Fig. 2 Schematic representation of air jet erosion tester

Figure 3 represents the morphology of alumina erodent, and Table 3 represents the parameters pertaining to solid particle erosion test.

Test samples are washed in acetone and weighed on a weighing scale with a 0.0001 mg resolution. The experiments were carried out by affixing the specimen to the specimen holder for 10 min with Alumina (Al₂O₃). The sample

Fig. 3 SEM images of **a** morphology of alumina (Al_2O_3) erodent and **b** EDS analysis

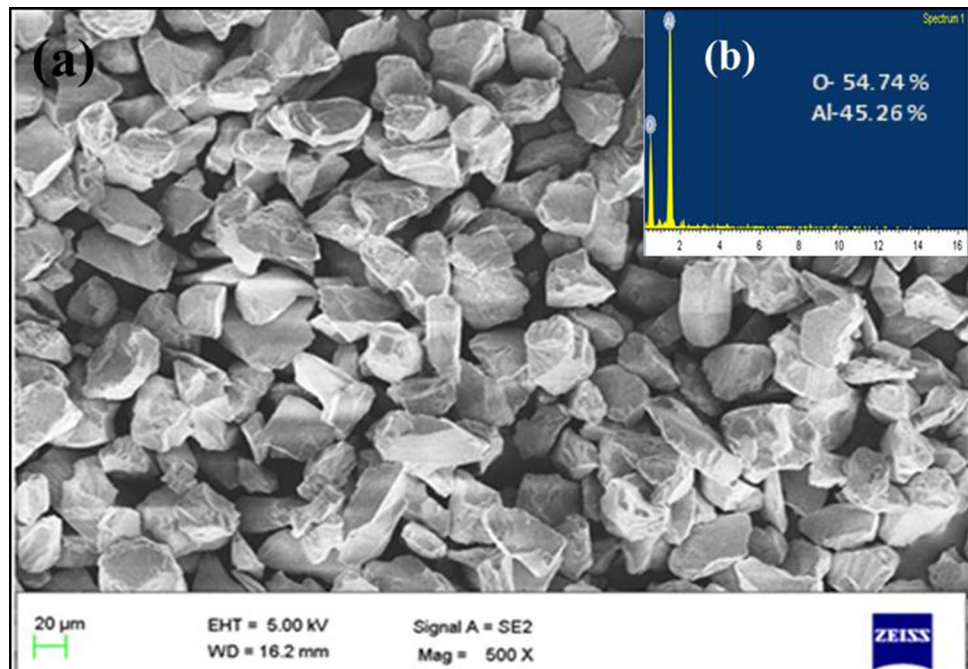


Table 3 Erosion test parameters

Erodent material	Alumina (Al_2O_3)
Average size	50 μm
Particle velocity	30 mts/s
Erodent feed rate	2 g/min
T time	10 min
D diameter of nozzle	1.5 mm
Standoff distance	10 mm

was weighing to determine the weight loss and repeat same procedure for 5 cycles. The erosion tests were conducted for three different temperatures of 300 °C, 500 °C and 700 °C and impact angles of 30° and 90°. The mass loss/erodent particle loss ratio is used to measure the erosion rate. The profilometer (Zeta instruments, 20, USA) is used to assess the volume loss of samples that have been exposed to erosion.

3 Results and Discussion

3.1 XRD Analysis

X-ray diffraction patterns of eroded samples at the different temperatures of 300 °C, 500 °C and 700 °C are shown in Fig. 4. The pattern looks slightly different at all the temperatures in Fig. 4. The WC-Co) + (Cr_3C_2 -NiCr)-coated sample at the temperature of 300 °C depicts the W_2C , Cr_{23}C_6 , NiWO_4 and NiCr_2O_4 phases as the major peaks, while Cr_3C_2

and Cr_2O_3 phases as minor peaks. At the temperature of 500 °C, the W_2C , Cr_{23}C_6 and NiWO_4 phases are identified as the major peaks and Cr_3C_2 , Cr_2O_3 and NiCr_2O_4 as minor peaks. Similarly, at the temperature of 700 °C, the W_2C , Cr_2O_3 and NiWO_4 are the major peaks and Cr_3C_2 , Cr_{23}C_6 and NiCr_2O_4 are the minor peaks. The decarburization of WC occurs during the plasma spray-coating process due to the higher temperatures, and it greatly transforms into the step of W_2C . Due to the mechanism of oxidation, the phases like W_2C , NiCr_2O_4 , NiWO_4 , Cr_2O_3 , Cr_3C_2 and Cr_{23}C_6 are observed at higher temperature of 700 °C. The oxides which are formed at higher temperature of 700 °C, improve erosion resistance of the coating, by forming a protective layer at the top surface of the coating.

3.2 Coating Structure and Property Analysis

Coating porosity value of (WC-Co) + (Cr_3C_2 -NiCr) is found to be the range of 2.5–3.5%. The average thickness value of coating is in the vicinity of 250 μm , composition on the coated surface shown in Fig. 5a, b and surface roughness of the coating is found to be 11.854 R_a . The measured value of (WC-Co) + (Cr_3C_2 -NiCr) coating's bond strength was found to be 16 MPa, and images of the coated samples after spallation during bond strength test are shown in Fig. 5c.

Average microhardness of the 35% (WC-Co) + 65% (Cr_3C_2 -NiCr) coating is found to be 538 HV. It is evident from Fig. 6 which shows that the value of the microhardness is found to be varied due to inhomogeneity in the coating structure and increasingly throughout. This may be due to

Fig. 4 X-ray of (WC-Co)+(Cr₃C₂-NiCr) coating at different temperatures of 300 °C, 500 °C and 700 °C

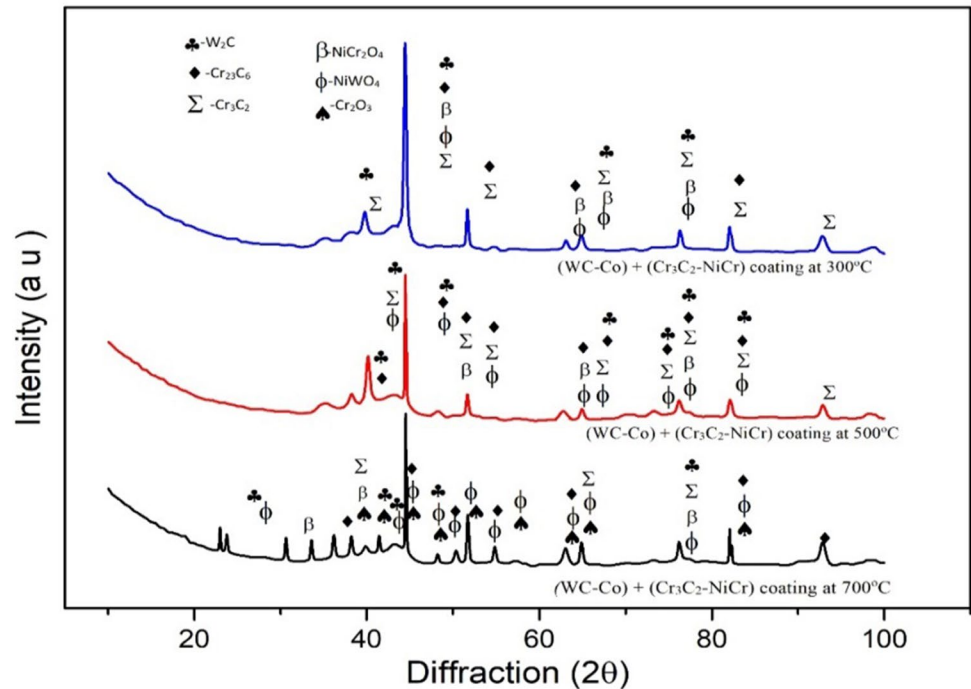
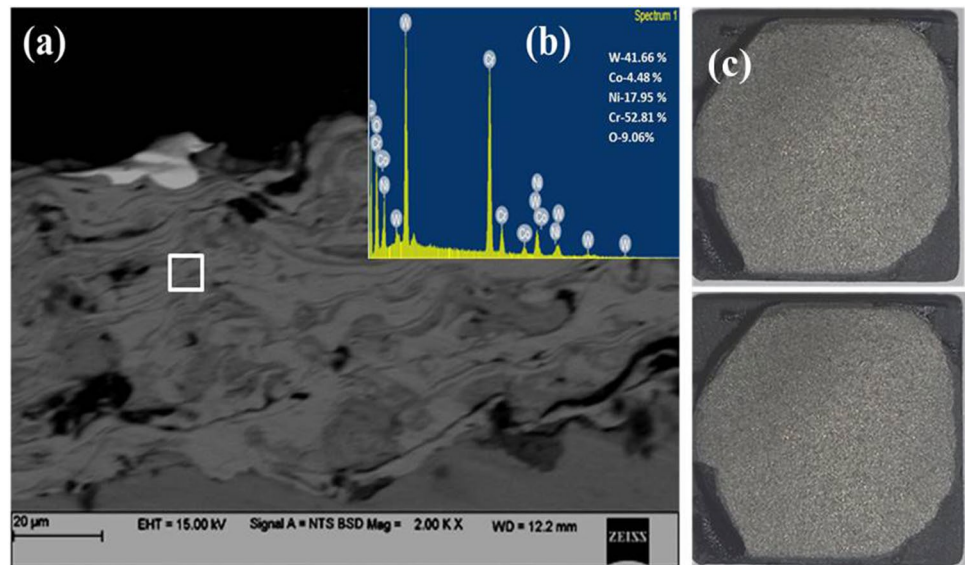


Fig. 5 Micrographs of **a** (WC-Co)+(Cr₃C₂-NiCr) coating, **b** coated samples before spallation during bond strength test, **c** coated samples after spallation during bond strength test



peening stress which is found at the grit blasting operation during the substrate preparation [14, 15].

3.3 Erosion Mechanism

Figure 7 shows the images of the erosion scars produced on MDN-420 alloy sample with 30° and 90° impact angles at the temperature of 700 °C. The scar which is eroded at the centre position represents a localized region of material removal which is indicated by “A” and surrounding zone which is elastically loaded is represented by “B”. The bar

chart indicates the volumetric erosion rate of the coating and the substrate as shown in Fig. 7(I). At 90° impingement, the volume erosion rate of the uncoated MDN-420 alloy is higher than at 30° for 300 °C temperature, which is standard behaviour of brittle materials where the material removal occurs predominantly by the chipping and cracking mechanism as shown in Fig. 7(I) and (II) [16]. Similarly, it is been observed from the bar chart that for 500 °C, the impingement at 90° is quite higher than that of 30°, indicating the brittle behaviour. At the 700 °C temperature, the impingement at 30° is higher than that 90° indicating the

Fig. 6 Microhardness profile of substrate and coating

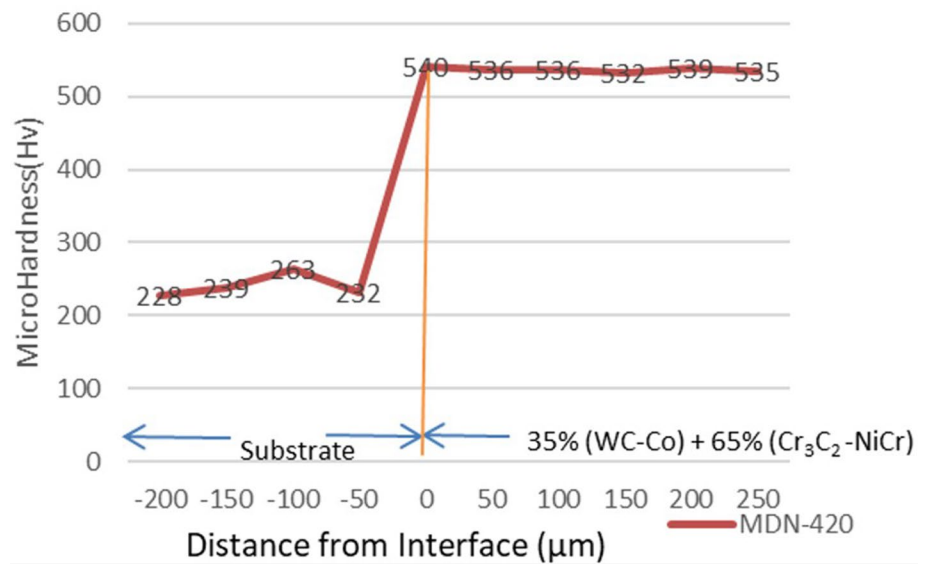
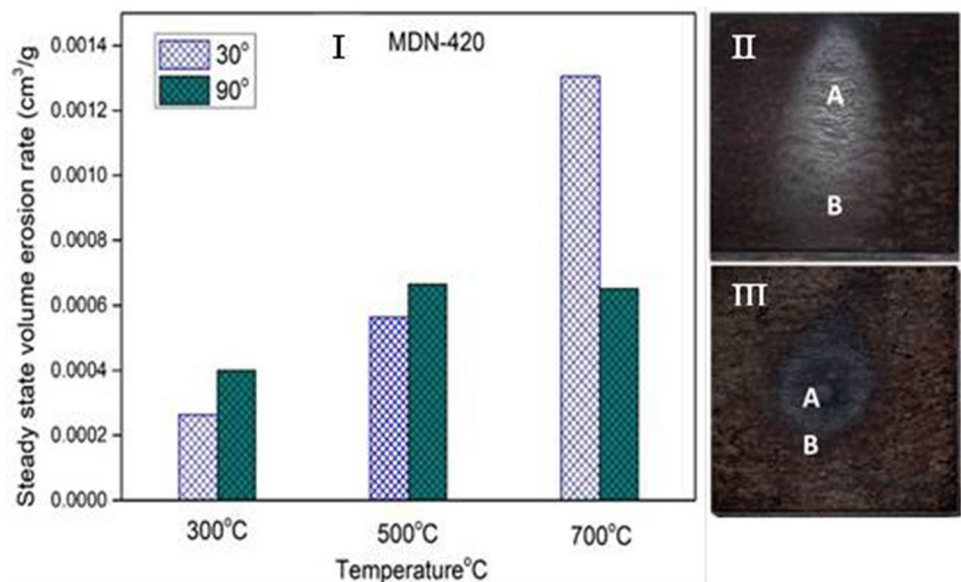


Fig. 7 Erosion rate of MDN-420 alloy (I) Steady-state volume erosion rate for 30° and 90° impact angles at 300 °C, 500 °C and 700 °C, Images of the erosion scars at 700 °C (II) 30° impact angle (III) 90° impact angle



ductile behaviour, it is clear from the above discussion that as the temperature increases from 300 °C to 700 °C, the erosion process switches from being purely brittle to being moderately ductile [17].

Figure 8a and b reveals the surface morphology of the MDN-420 steel surface eroded at 700 °C with impact angle of 30°. From the micrographs Fig. 8a, it is clear from the material; the lips and grooves are formed with severe plastic deformation. As the same feature is explained by the author Ramesh et al., such ductile extrusion of the material may have predominantly occurred in the softer nickel-based metallic binder matrix [18]. From the micrograph Fig. 8b, it can be observed that large ploughs are formed with the length of few micrometres with subsequent fracture

by the impacting particles. Even the small ploughs are also observed. Figure 8c and d reveals the surface morphology of the MDN-420 steel surface eroded at 700 °C with impact angle of 90°. From the micrograph, Fig. 8c shows evidence of the Al_2O_3 particles embedded on the groove surface, which is formed due to the mechanism of erosion [19]. In Fig. 8d, the larger ploughs and the small craters can be seen due to the subsequent impacts of the alumina erodent on the surface, indicating the common feature of ductile erosion mode.

Figure 9 shows the images of the erosion scars produced on (WC-Co) + (Cr₃C₂-NiCr)-coating sample with 30° and 90° impact angle at the temperature of 700 °C. The scar which is eroded at the centre position represents a localized

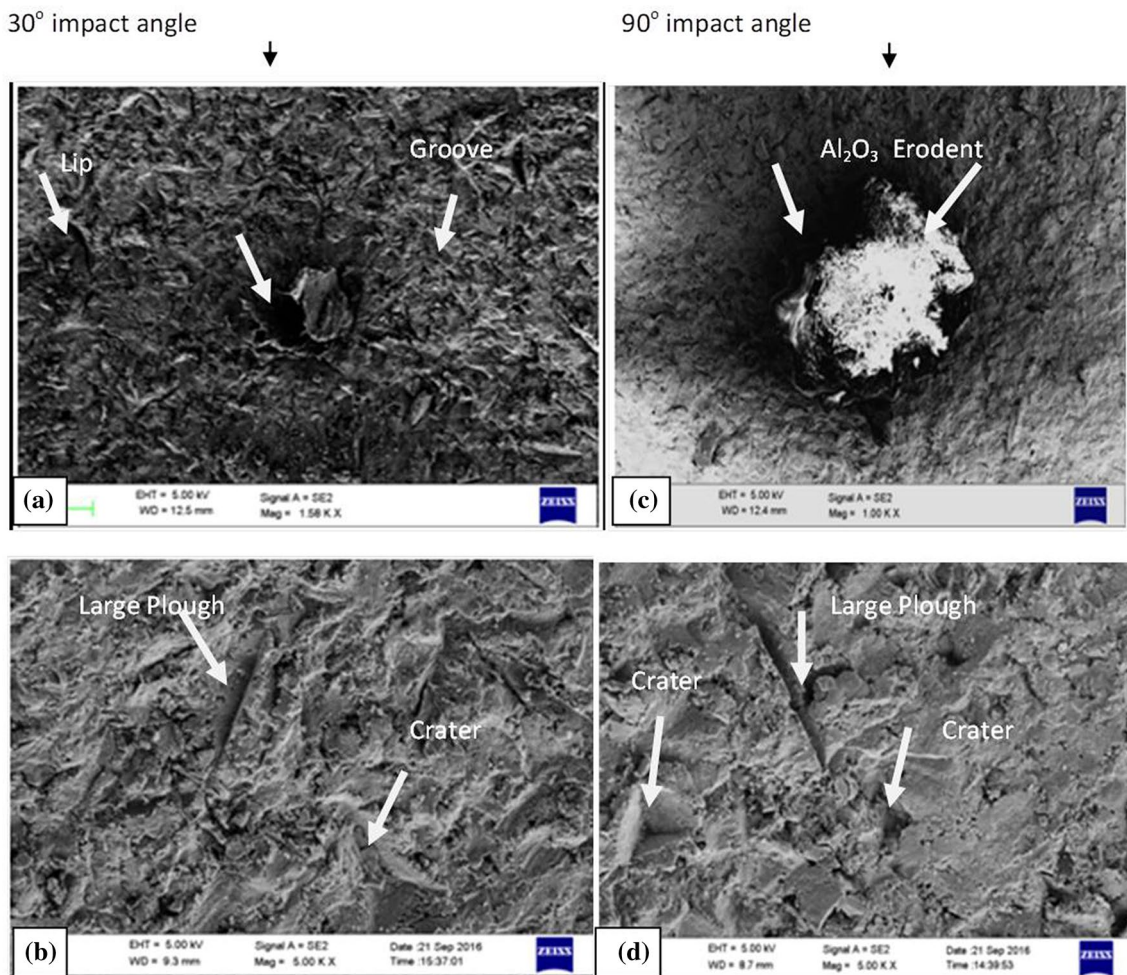
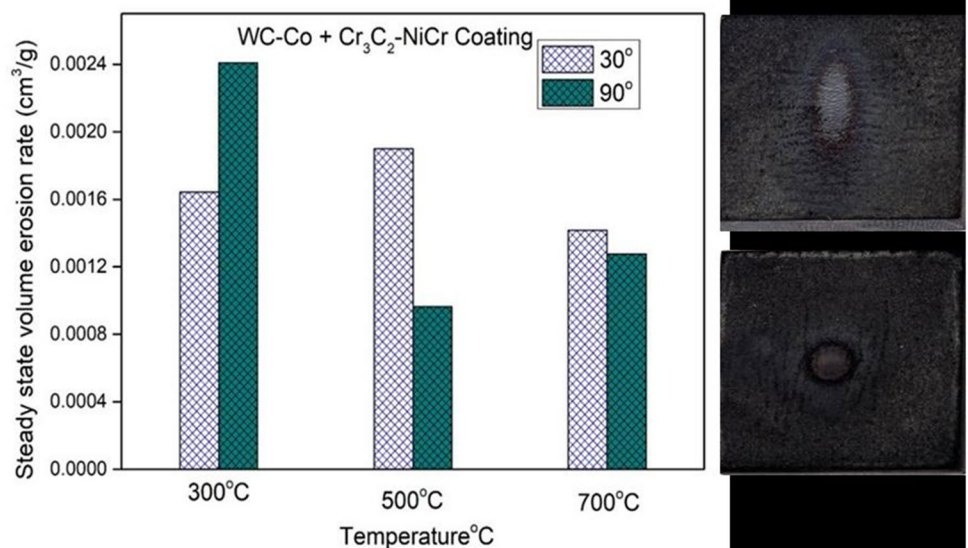


Fig. 8 SEM images showing the erosion surface morphology of MDN-420 alloy at 700 °C with impact angles of 30° and 90° **a** and **b** images showing the eroded surface at 30° impact angle. **c** and **d** images showing the eroded surface at 90° impact angle

Fig. 9 Erosion rate of (WC–Co)+(Cr₃C₂–NiCr) coating impacted by alumina erodent at 700 °C (I) Steady-state volume erosion rate for 30° and 90 ° impact angles at 300 °C, 500 °C, and 700 °C, Images of the erosion scars at 700 °C (II) 30° impact angle (III) 90° impact angle



region of material removal which is indicated by “A” and surrounding zone which is elastically loaded is represented by “B”. The brittle behaviour of the coating [20] for the temperature 300 °C is observed from the bar chart. It is clearly indicating that, volume erosion rate for the coating is higher at 90° when compared with 30° of impingement angle. For the temperature 500 °C, it is observed from the bar chart that the impingement at 30° is higher than that 90°. Similarly for the 700 °C temperature, the impingement at 30° is higher than that 90°. For both the temperatures 500 °C and 700 °C at 30° and 90° impingement angles, the (WC–Co) + (Cr₃C₂–NiCr) coating implies the ductile behaviour. It is clear from the above discussion that as the temperature increases from 300 to 700 °C, the erosion resistance of the coating increases. Mahantayya et al. (2017) reported that plasma spraying has been successfully used to develop NiCrAlY-25WC-Co/Cenosphere coating. Erosion resistance of developed coating increases with increasing temperature for 30° impact angle. At elevated temperature, erosion resistance of coating is 71% higher than MDN 321 steel substrate. Similar results are explained by the author Guan-Jun Yang et al. [21–23]. This effect may be due to softening of the material which results in increase of ductility as the temperature increases and further prevents from cracking which in turn improves the erosion resistance of the coating.

Under the similar test conditions, the special steel alloy MDN-420 exhibits the lesser wear loss when compared to (WC–Co) + (Cr₃C₂–NiCr) coating. This condition is due to the shielding effect of alumina particles which are implanting on the surface of the substrate, which avoids the further material loss to occur. The ratio of erodent particle hardness (Hp) to target hardness (Ht) is well known to have a regulating effect on erosion mechanisms [24–26]. The average hardness value of the Al₂O₃ erodent used in this present work is 886 HV and, for the MDN-420 alloy, the average hardness value is 232 HV. As compared to (WC–Co) + (Cr₃C₂–NiCr) coating, the Hp/Ht ratio is approximately 3.8, allowing alumina particles to penetrate the target substrate material, serving as a barrier against impacting particles, resulting in less wear loss of MDN-420 alloy. Only if Hp/Ht > 1.2, erodent abrasive particles of any form will cause plastic scratching and indent the surface [18]. The embedment of alumina particle in the eroded surface of MDN-420 alloy is clearly visible (Fig. 9), and the erosion process basically involves indentation caused by extreme plastic deformation. Sidhu et al. [19] and Mishra et al. [27] also explained about the silica particle embedment on super alloys and steels.

Figure 10a and b reveals the surface morphology of the 35%(WC–Co) + 65% (Cr₃C₂–NiCr)-coating surface eroded at 700 °C with impact angle of 30°. From the micrograph 10a, it can be clearly observed that the

small tearing is formed due to the repeated impact of the erodent. The erodent particles deform the surface by the tearing. The alumina erodent particles deform the surface by the mechanism of ploughing, displacing material to the side and in front of the particle in the shape of a lip due to the extreme plastic flow, as shown in micrograph 10b. Figure 10c and d indicates the surface morphology of the (WC–Co) + (Cr₃C₂–NiCr)-coating surface eroded at 700 °C with impact angle of 90°. The morphology indicates the grooves formed in the nickel-rich binder matrix, which is characterized by the crater which is formed by the mechanism of ploughing and lips at the rim of the crater are clearly visible in the micrograph (Fig. 10c). It is also observed that sharp-edged alumina particles which are incrustated in the surface, forming the crater, extrude as micro-platelets at the site of impacts. These platelets of metal that are locally attached to the crater rim are further forged by the subsequent impact of the erodent and will be strained to their critical plastic strain. From Fig. 10d, it can be observed that the coating is severely plastically deformed. The strain localization is a feature, which is commonly seen in ductile erosion behaviour, and is indicated by the pull-out regions surrounded by craters and protuberant lips [28]. Figure 10e, f shows the EDS of the (WC–Co) + (Cr₃C₂–NiCr) coating eroded at 700 °C with impact angle of 90° confirming the nickel-rich binder matrix.

4 Conclusion

1. Plasma spray coating has been successfully used to deposit the 35% (WC–Co) + 65% (Cr₃C₂–NiCr) coating on to the MDN-420 alloy with porosity of 2.5 to 3.5% and the hardness value of 538 HV.
2. The erosion resistance of the coating increases with the increase in the temperature from 300 to 700 °C for both the 30° and 90° impact angles.
3. The (WC–Co) + (Cr₃C₂–NiCr) coating shows the ductile erosive mechanism at the temperatures of 500 °C and 700 °C where in material, removal is occurred with the formation of craters and lips followed by the severe plastic deformation. At lower temperature of 300 °C, the coating exhibits the brittle erosive mechanism.
4. MDN-420 steel exhibits the lesser wear loss when compared to the (WC–Co) + (Cr₃C₂–NiCr)-coated alloy. This is due to embedment of the alumina particles on substrate surface, which creates the shielding effect and prevents the further material loss to occur.

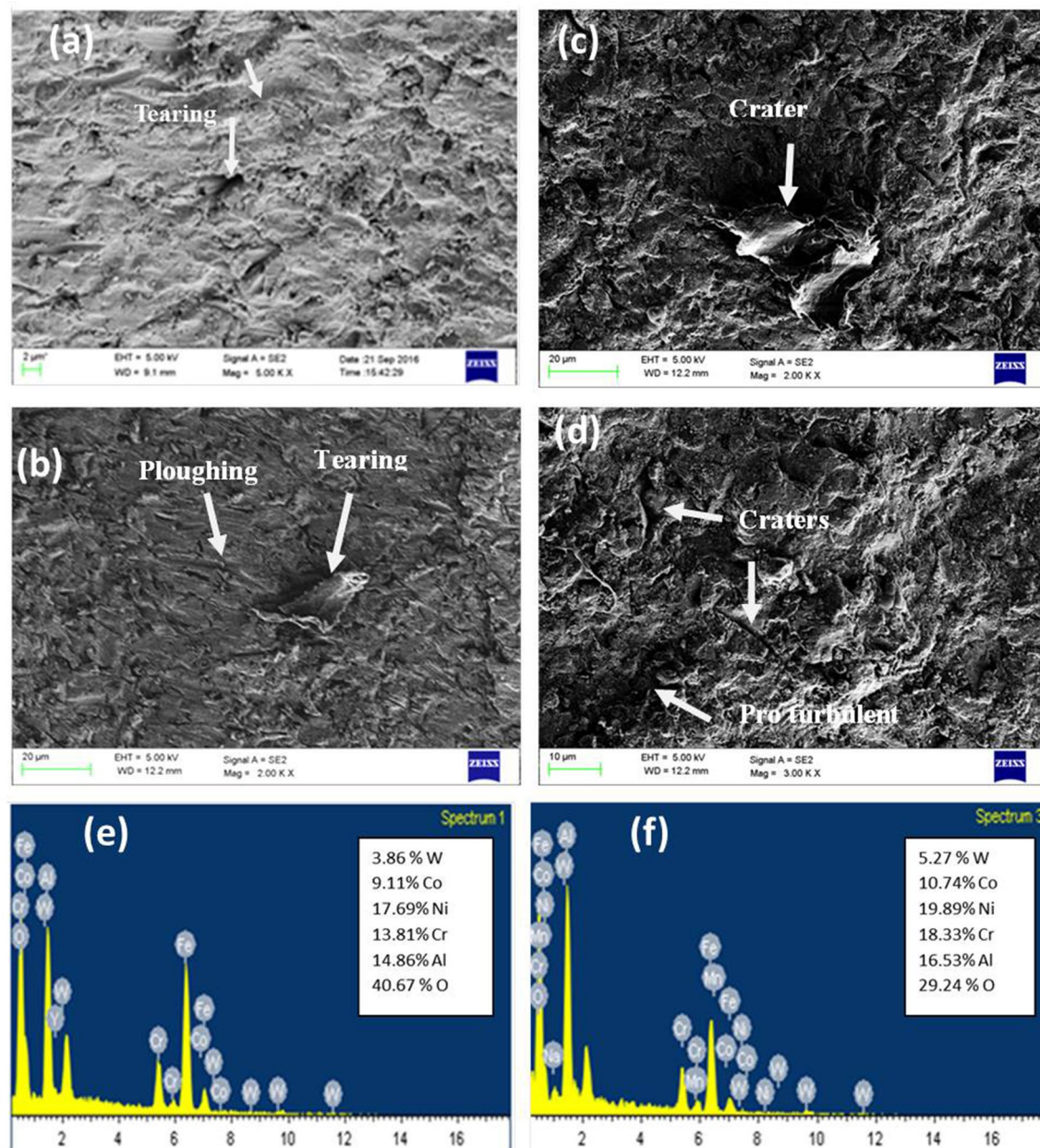


Fig. 10 SEM images showing the erosion morphology of (WC–Co)+(Cr₃C₂–NiCr) coating at 700 °C with impact angles of 30° and 90°. **a** and **b** Images of eroded surface at 30° impact angle. **c** and **d** Images show the eroded surface at 90° impact angle

Funding This research received no specific grant from any funding agency.

Declarations

Conflict of interest On behalf of all authors, the corresponding author states that there is no competing of interest.

References

1. Chawla V, Chawla A, Puri D, Prakash S, Gurbuxani PG, Sidhu BS (2011) Hot corrosion & erosion problems in coal based power plants in India and possible solutions—a review. *J Miner Mater Charact Eng* 10(04):367
2. Sundararajan G (1995) The solid particle erosion of metallic materials: the rationalization of the influence of material variables. *Wear* 186:129–144
3. Doddamani M, Mathapati M, Ramesh MR (2018) Microstructure and tribological behavior of plasma sprayed NiCrAlY/WC-Co/cenosphere/solid lubricants composite coatings. *Surf Coat Technol* 354:92–100

4. El Rayes MM, Abdo HS, Khalil KA (2013) Erosion-corrosion of cermet coating. *Int J Electrochem Sci* 8(1):1117–1137
5. Praveen AS, Sarangan J, Suresh S, Subramanian JS (2015) Erosion wear behaviour of plasma sprayed NiCrSiB/Al₂O₃ composite coating. *Int J Refract Metal Hard Mater* 52:209–218
6. Chatha SS, Sidhu HS, Sidhu BS (2012) Characterisation and corrosion-erosion behaviour of carbide based thermal spray coatings. *J Miner Mater Charact Eng* 11(6):569–586
7. Chatha SS, Sidhu HS, Sidhu BS (2012) Characterisation and corrosion-erosion behaviour of carbide based thermal spray coatings. *J Miner Mater Charact Eng* 11(06):569
8. Di Girolamo G, Brentari A, Blasi C, Serra E (2014) Microstructure and mechanical properties of plasma sprayed alumina-based coatings. *Ceram Int* 40(8):12861–12867
9. Zavareh MA, Sarhan AADM, Zavareh PA, Abd Razak BB, Basirun WJ, Ismail MBC (2016) Development and protection evaluation of two new, advanced ceramic composite thermal spray coatings, Al₂O₃-40TiO₂ and Cr₃C₂-20NiCr on carbon steel petroleum oil piping. *Ceram Int* 42(4):5203–5210
10. Nithin HS, Desai V, Ramesh MR (2017) An investigation on high temperature erosion behaviour of plasma sprayed CoCrAlY/Al₂O₃/YSZ on Fe and Ni based alloys. *Pertanika J Sci Technol* 25(2):397–406
11. Reddy M, Prasad CD, Patil P, Ramesh MR, Rao N (2021) Hot corrosion behavior of plasma-sprayed NiCrAlY/TiO₂ and NiCrAlY/Cr₂O₃/YSZ cermets coatings on alloy steel. *Surf Interfaces* 22:100810
12. Prasanna ND, Siddaraju C, Shetty G (2018) Studies on the role of HVOF coatings to combat erosion in turbine alloys. *Mater Today* 5(1):3130–3136
13. Madhu Sudana Reddy G, Ramesh MR, Rao N, Jegadeeswaran N (2018) Corrosion of metal construction structures. *Int J Mech Prod Eng Res Dev* 8(6):227–237
14. Wani TP, Raja R, Reddy G (2021) Synthesis and mechanical properties of HDPE based nano-clay polymer composites for industrial applications. *Adv Mater Process Technol*. <https://doi.org/10.1080/2374068X.2021.1896864>
15. Somasundaram B, Kadoli R, Ramesh MR, Ramesh CS (2016) High temperature corrosion behaviour of HVOF sprayed WC-CrC-Ni coatings. *Int J Surf Sci Eng* 10(4):400–413
16. Singh A, Goyal K, Goyal R, Krishan B (2021) Hot corrosion behaviour of different ceramics coatings on boiler tube steel at 800 °C temperature. *J Bio-and Tribo-Corrosion* 7(1):1–9
17. Levy AV, Buqian W (1988) Erosion of hard material coating systems. *Wear* 121(3):325–346
18. Wang Y, Yang Y, Yan MF (2007) Microstructures, hardness and erosion behavior of thermal sprayed and heat treated NiAl coatings with different ceria. *Wear* 263(1–6):371–378
19. Ramesh MR, Prakash S, Nath SK, Sapra PK, Venkataraman B (2010) Solid particle erosion of HVOF sprayed WC-Co/NiCr-FeSiB coatings. *Wear* 269(3–4):197–205
20. Ramachandran CS, Balasubramanian V, Ananthapadmanabhan PV (2013) Erosion of atmospheric plasma sprayed rare earth oxide coatings under air suspended corundum particles. *Ceram Int* 39(1):649–672
21. Wang B-Q, Verstak A (1999) Elevated temperature erosion of HVOF Cr₃C₂/TiC-NiCrMo cermet coating. *Wear* 233–235:342–351
22. Yang GJ, Li CJ, Zhang SJ, Li CX (2008) High-temperature erosion of HVOF sprayed Cr₃C₂-NiCr coating and mild steel for boiler tubes. *J Therm Spray Technol* 17(5):782–787
23. Mathapati M, Ramesh MR, Doddamani M (2017) High temperature erosion behavior of plasma sprayed NiCrAlY/WC-Co/cenosphere coating. *Surf Coat Technol* 325:98–106
24. Ndumia JN, Kang M, Gbenontin BV, Lin J, Nyambura SM (2021) A review on the wear, corrosion and high-temperature resistant properties of wire arc-sprayed Fe-based coatings. *Nanomaterials* 11(10):2527
25. Hearley JA, Little JA, Sturgeon AJ (1999) The erosion behaviour of NiAl intermetallic coatings produced by high velocity oxy-fuel thermal spraying. *Wear* 233:328–333
26. Hussainova I, Kubarsepp J, Pirso J (2001) Mechanical properties and features of erosion of cermets. *Wear* 250(1–12):818–825
27. Mahesh RA, Jayaganthan R, Prakash S (2009) Microstructural characteristics and mechanical properties of HVOF sprayed NiCrAl coating on superalloys. *J Alloy Compd* 468(1–2):392–405
28. Mishra SB, Chandra K, Prakash S, Venkataraman B (2006) Erosion performance of coatings produced by shrouded plasma spray process on a Co-based superalloy. *Surf Coat Technol* 201(3–4):1477–1487

Publisher's Note Springer Nature remains neutral with regard to jurisdictional claims in published maps and institutional affiliations.